ELSEVIER

Polymer 40 (1999) 5907–5917

polymer

Miscible binary blends of poly(ethylene oxide) and poly(ether sulphone). Part 1: crystallization kinetics, morphology and thermal behavior

G. Dreezen[a], Z. Fang[b], G. Groeninckx[a,*]

[a]*Catholic University of Leuven (KULeuven), Department of Chemistry, Laboratory of Macromolecular Structural Chemistry, Celestijnenlaan 200F, 3001 Heverlee, Belgium*

[b]*Hangzhou University, Department of Chemistry, Hangzhou 310028, People's Republic of China*

Received 24 August 1998; received in revised form 3 November 1998; accepted 3 November 1998

Abstract

The isothermal crystallization kinetics, semi-crystalline morphology and thermal behavior of poly(ethylene oxide) (PEO) in miscible binary blends with an amorphous component, poly(ether sulphone) (PES), were investigated below LCST by means of optical microscopy, differential scanning calorimetry and small angle X-ray scattering. Addition of PES to PEO reduces both the overall crystallization rate and the spherulite growth rate of PEO. The change of the nucleation regime and an Avrami analysis of the crystallization kinetics are discussed. The double melting behavior of PEO in blends with PES is attributed to both secondary crystallization and recrystallization during heating. A change in the supermolecular structure from intermediate spherulite-hedrite to spherulite appears on blending PEO with PES. The segregation behavior of amorphous PES during crystallization of PEO is investigated.

Keywords: Miscible PEO/PES blends; Crystallization kinetics; Melting behavior

1. Introduction

The presence of different thermodynamic phase transitions such as liquid–liquid phase separation, homogenization or crystallization in binary polymer blends often results in a complex phase diagram. When these phase transitions compete kinetically, a variety of blend morphologies can be created. Several authors [1–3] have introduced the concept of structure formation by liquid–liquid phase separation in competition or followed by crystallization in these systems; however until now only a few studies on binary blends with a LCST-type demixing behavior have been performed [4–11]. The present study deals with blends of one crystallizable and one amorphous component with a lower critical solution temperature.

Blends of poly(ethylene oxide) (PEO) and poly(ether sulphone) (PES) are miscible over the whole composition range up to 75°C. At this temperature a lower critical solution behavior has been reported [12,13]. The kinetics of phase separation of a 90/10 PEO/PES blend was investigated experimentally and also predicted by use of the Cahn–Hilliard theory [13]. Prior to the study of the crystallization after a phase separation process, it is of crucial importance to thoroughly understand the crystallization kinetics, melting behavior and semi-crystalline morphology in the completely miscible state below the cloud point curve.

The crystallization kinetics, morphology and thermal behavior of PEO in completely miscible binary blends with the amorphous components PMMA, PEMA, PVPh, PVAc have been studied by Martuscelli et al. [14–18]. The influence of the amorphous component on the crystallization behavior of PEO depends on the molecular weight of this component, the presence of specific interactions and the glass-transition temperature of the blend. An empirical equation describing the spherulite growth rate in blends of a crystallizable and an amorphous component was developed by Alfonso and Russell [19] based on measurements of the spherulite growth rate in PEO/PMMA blends. The segregation behavior of the amorphous component during crystallization of PEO in binary blends with different types of interactions and different glass-transition temperatures has recently been investigated [20]. The crystallization, melting and semi-crystalline structure of blends of PEO with an amorphous aromatic polyamide (Aramide 34I) with a high glass-transition temperature of 225°C have also been studied [21].

The present article is the first study on the crystallization, thermal behavior and morphology of PEO/PES blends. The influence of PES on the crystallization kinetics of PEO has

* Corresponding author. Tel.: +32 16 32 74 40; fax: +32 16 32 74 90.

0032-3861/99/$ - see front matter
PII: S0032-3861(98)00809-X

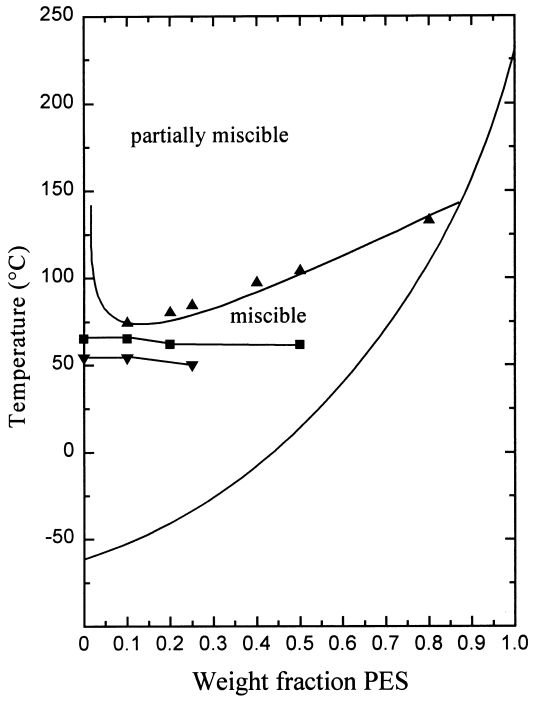

Fig. 1. Phase diagram of PEO/PES blends: (▲) cloud point curve, (■) melting temperature T_m, (▼) upper isothermal crystallization temperature T_c, (—) glass-transition temperature T_g.

been studied and related to the observed melting phenomena. The supermolecular structure of the blends resulting from the crystallization of PEO and the segregation behavior of PES are investigated.

2. Experimental

2.1. Materials and blend preparation

Poly(ethylene oxide) obtained from UCB with a viscosity average molecular weight ($\bar{M}_v$) of 17000 g/mole and a polydispersity of 1.35 was blended with Poly(ether sulphone) (trade name Victrex 4800G) obtained from Victrex Limited (UK) with a viscosity average molecular weight ($\bar{M}_v$) of 61000 g/mole and a polydispersity of 1.72. PEO/PES blends of wt/wt compositions 100/0, 90/10, 80/20, 75/25 and 50/50 were obtained by preparing 10% solutions of both components in dimethylformamide (DMF), mixing the solutions in appropriate compositions and removal of the solvent under vacuum at 70°C. The blends were additionally dried under vacuum for 2 days at 60°C. Prior to the experiments the samples were kept at 60°C under vacuum for 12 h.

2.2. Optical microscopy

Cloud points were detected from the light transmitted by thin samples placed between cover glasses under an OLYMPUS optical microscope coupled with a computer controlled CCD-camera. The same device was used to measure the spherulite growth rates of PEO in the blends. At different times during the growth process, images of the sample were stored with the polarizers under 45°. The spherulite growth rate was calculated from the increase of the spherulite radius with time for all blends that crystallized over a reasonable time (5 h) at temperatures between 15°C and 55°C. The resulting supermolecular structure was investigated using the microscope with crossed polarizers.

2.3. Differential scanning calorimetry

A Perkin-Elmer DSC7 differential scanning calorimeter was used to investigate the overall kinetics of isothermal crystallization. The samples were kept for 5 min at 75°C and cooled to the crystallization temperature T_c at a rate of 40°C/min. The weight fraction X_t of material crystallized at time t was calculated from the ratio of the crystallization enthalpy generated at time t to the crystallization enthalpy of a completely crystallized sample.

The DSC-melting behavior was investigated at a heating rate of 10°/min. For the investigation of the recrystallization process different heating rates from 1.5°/min to 40°/min were used; these measurements were normalized to a heating rate of 1°/min and corrected for the temperature shift of an indium calibration sample. The crystallinity was determined from the DSC melting curves according to the method of Mathot et al. [22]. The advantage of this method is that the crystallinity does not depend on the definition of an arbitrary baseline under the melting peak, but yields an analyst-independent determination of the transition enthalpy via an area determination with a baseline extrapolated from the melt. The crystallinity as function of temperature during cooling or heating is determined from:

$$X_c(T) = \frac{[A_2 - A_1]_T}{\Delta h(T)} \quad (1)$$

where $(A_2 - A_1)_T$ is the transition enthalpy. The temperature dependent enthalpy function $\Delta h(T) = h_a(T) - h_c(T)$ is available from the ATHAS databank [23,24] for several types of semi-crystalline polymers.

2.4. Small angle X-ray scattering

SAXS-measurements were performed using a Rigaku-type Kratky camera with infinite slit geometry on 2 mm thick PEO/PES blend samples isothermally crystallized within 60 min at 44°C. Ni-filtered Cu Kα radiation was produced using a Rigaku rotating anode device (12 kW) operated at 40 kV and 50 mA. Scattering patterns were collected with a linear position sensitive detector (Braun OED-SOM). The data analysis was performed using the FFSAXS-5 [25] program (adapted for pc) as developed by Vonk. The smeared intensity $I_3(s)$ was obtained after correction for the background scattering; subsequent desmearing yields the corresponding pinhole intensity $I_3(s)$. Lorentz correction was applied by multiplying $I_3(s)$ by s^2 in order to obtain a one-dimensional intensity profile $I_1(s)$.

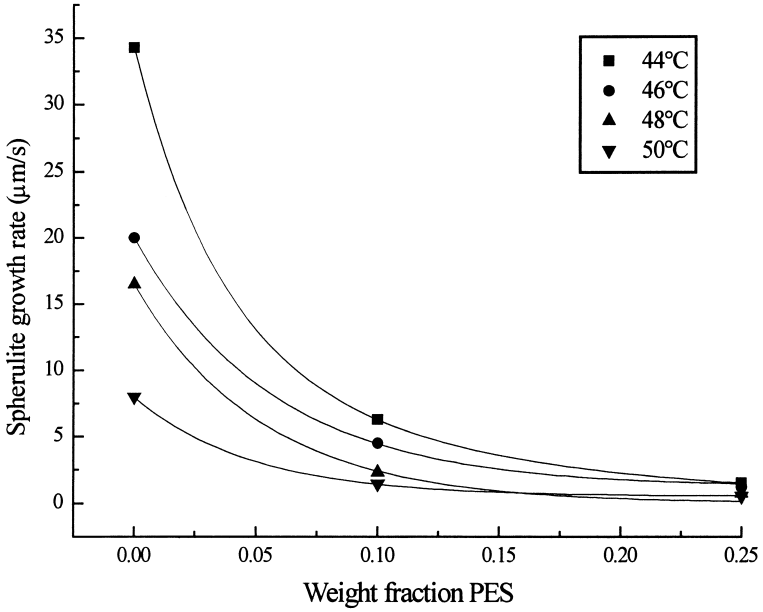

Fig. 2. Spherulite growth rate versus weight fraction amorphous component PES at different isothermal crystallization temperatures (44°C, 46°C, 48°C and 50°C).

3. Results and discussion

The phase diagram of PEO/PES blends is presented in Fig. 1; the system exhibits a temperature and composition dependent miscibility. The blends are miscible over the whole composition range up to 75°C; above this temperature a LCST-type demixing behavior is present. The crystallization curve (T_c) indicates the upper limit where PEO/PES blends crystallize completely within 5 h. Isothermal crystallization for long periods revealed that PEO crystallizes in blends up to 50 wt.% of PES. The melting point curve (T_m) represents the melting temperatures of these samples. The glass-transition temperature T_g of the blends, as calculated from the Fox-equation [26], changes rapidly with increasing PES content. All experiments considered here were started from the one-phase miscible region below the cloud point curve.

3.1. Spherulite growth kinetics and secondary nucleation regime

The spherulite growth rate of crystallizable

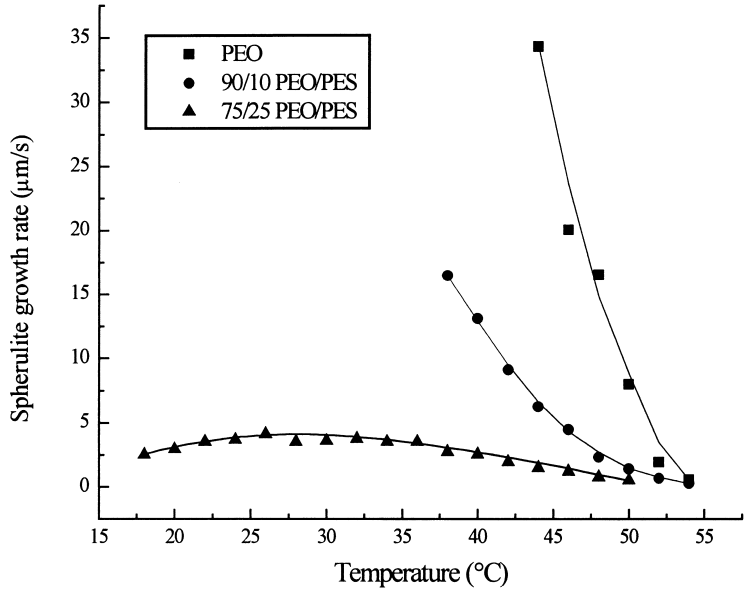

Fig. 3. Spherulite growth rate as a function of crystallization temperature for 100/0, 90/10 and 75/25 PEO/PES blends.

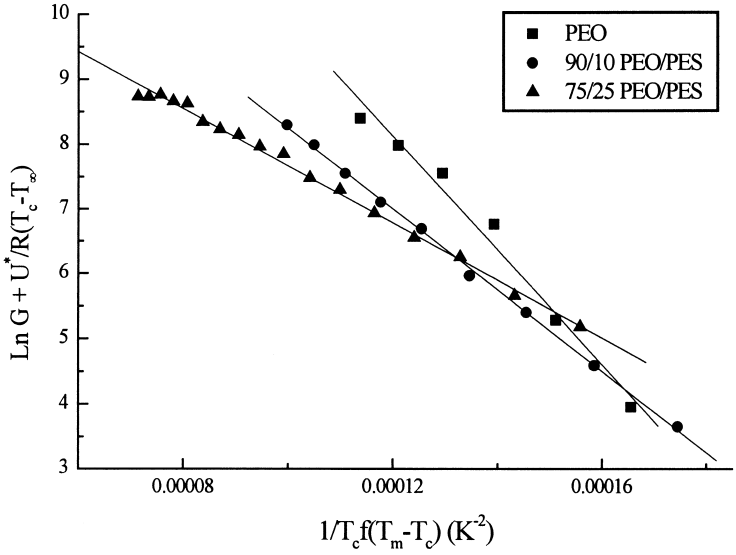

Fig. 4. Plot of ln $G + U^*/R(T_c - T_\infty)$ versus $(1/T_c)f(T_m - T_c)$ for 100/0, 90/10 and 75/25 PEO/PES blends. From the slope of the linear fit the secondary nucleation term K_g is determined.

homopolymers has been described in the past using a modified version [27] of the phenomenological nucleation theory of Turnbull and Fisher [28]. The spherulite growth rate G depends on the free energy required to form a critical nucleus on the crystal surface (ΔF^*) (secondary nucleation) and the energy necessary to transport chain segments across the liquid–solid interface:

$$G = G_0 \exp\left[\frac{-\Delta E}{RT_c}\right] \exp\left[\frac{-\Delta F^*}{k_b T_c}\right] \quad (2)$$

where G_0 is a growth rate constant, T_c the crystallization temperature, R the gas constant and k_b the Boltzmann constant. The spherulite growth rate of a crystallizable component (G_{bl}) in miscible blends with an amorphous component, as derived from the phenomenological approach of Alfonso and Russell [19], is given by:

$$G_{bl} = \frac{\varphi_2 k_1 k_2}{k_1 + k_2} \exp\left[\frac{-\Delta F_{bl}^*}{k_b T_c}\right] \quad (3)$$

where φ_2 represents the volume fraction of the amorphous component, k_1 the transport rate of the crystalline segments to the liquid–solid interface and k_2 the diffusion rate of the amorphous component away from the growth front. The approach of Alfonso and Russell takes into account the specific interactions between the blend components, the diffusion of the amorphous component, the blend T_g and the dilution of the crystallizable component. According to this theory a bell-shaped curve is obtained for the spherulite growth rate as a function of temperature; the growth rate is nucleation-controlled at low degrees of undercooling and diffusion-controlled at higher degrees of undercooling.

The spherulite growth rate of PEO in PEO/PES blends as a function of the weight fraction PES at different crystallization temperatures is presented in Fig. 2. The growth rate decreases as the concentration of PES increases and the crystallization of PEO is inhibited above 50 wt.% of PES. The change of the spherulite growth rate with the crystallization temperature can be seen in Fig. 3. From 50°C towards lower crystallization temperatures the spherulite growth rate increases for all PEO/PES blend compositions studied. At high degree of undercooling, pure PEO and the 90/10 PEO/PES blend start to crystallize before the isothermal crystallization temperature is reached and no additional data points can be obtained. For the 75/25 PEO/PES blend, the spherulite growth rate exhibits a maximum at about 28°C. Above 28°C the growth rate is predominantly nucleation controlled; below 28°C it is diffusion controlled.

The decrease of the spherulite growth rate of PEO in the PEO/PES blends is larger than in the miscible blends with the amorphous components PMMA, PEMA, PVAc and EVAc [14–18,29–31], that all have a glass-transition temperature far below that of PES. In PEO/Aramide 34I blends [21], the decrease of the spherulite growth rate is even stronger than in PEO/PES blends. Both amorphous components PES and Aramide 34I have the same glass-transition temperature (225°C) but Aramide 34I forms, in contrast with PES, hydrogen bonds with PEO. The mobility of PEO-chains decreases in blends with these high T_g amorphous components and is the determining factor in the decrease of the spherulite growth rate in blends with a small amount of PES. The specific intermolecular interactions play a secondary role, but account for the stronger decrease of the spherulite growth rate of PEO in blends with Aramide 34I than in blends with PES.

From the spherulite growth rate data the secondary nucleation regime can be evaluated. Eq. (2) can be rewritten in terms of an activation energy U^* required for transport of segments across the liquid–solid interface and a nucleation

Table 1
Spherulite growth rate, nucleation term K_g and nucleation regime of PEO/PES blends

PEO/PES composition	T_c (°K)	G (μm/s)	Nucleation regime	K_g (K^2)
100/0	327	0.5	II	87739
	325	1.9		
	323	7.9		
	321	16.4		
	319	24		
	317	34.2		
90/10	327	0.3	II	62322
	325	0.7		
	323	1.4		
	321	2.3		
	319	4.4		
	317	6.2		
	315	9.1		
	313	13.1		
	311	16.4		
75/25	323	0.5	III	44229
	321	0.7		
	319	1.2		
	317	1.5		
	315	1.9		
	313	2.5		
	311	2.7		
	309	3.5		
	307	3.5		
	305	3.7		
	303	3.6		
	301	3.5		
	299	4.1		
	297	3.7		
	295	3.5		
	293	2.9		
	291	2.5		

term K_g describing the secondary nucleation process [27]:

$$\ln G + \frac{U^*}{R(T_c - T_\infty)} = \ln G_0 - K_g\left(\frac{1}{f\,T_c\Delta T}\right) \quad (4)$$

where $U^* = 4120$ cal/mole [27], $T_\infty = T_g - 51.3$, $\Delta T = T_m^0 - T_c$, $f = 2T_c/(T_c + T_m)$, $K_g = 2jb\sigma\sigma_e T_m^0/f\Delta h_f k_b$ with $\sigma\sigma_e$ the product of the lateral and fold surface free energy, Δh_f is the heat of fusion (196.4 J/g) [23,24], b is the thickness of a monomolecular layer (4.65 Å) and T_m^0 is the equilibrium melting temperature of PEO (73°C), j is a constant 1 for nucleation regime I, 2 for nucleation regime III. A plot of the left-hand side term of Eq. (4) versus $1/fT_c\Delta T$ allows to calculate the nucleation term K_g from the slope of the straight lines obtained, and is presented in Fig. 4 for the 100/0, 90/10 and 75/25 PEO/PES blends. The growth rate data are summarized in Table 1. Interpretation of the crystallization process in terms of the nucleation regime (I, II or III), as described by Lauritzen and Hoffman [32], is possible from K_g. One defines a parameter Z as:

$$Z = 10^3\left(\frac{l}{2b}\right)\exp\left(\frac{-X}{T_c\Delta T}\right) \quad (5)$$

where l is the lamellar thickness. When $X = K_g$ and $Z \leq 0.01$, crystallization occurs according to regime I in which a secondary nucleus formed on the crystallizing lamellar surface rapidly completes the layer. When $X = 2K_g$ and $Z \geq 1$, crystallization occurs according to regime III where many new secondary surface nuclei form before the lamellar layer is completed. In all other cases the intermediate regime II is followed. The lamellar thickness was estimated from data of Arlie et al. [33] and gave a satisfactory agreement with the few data points in our study. K_g and the results on the nucleation regime are summarized in Table 1.

Pure PEO and the 90/10 PEO/PES blend crystallize according to the intermediate crystallization regime II where the formation of secondary nuclei competes with the completion of the crystalline lamellar surface. From an amount of 25 wt.% amorphous component the crystallization process is controlled by regime III where nuclei are formed in large numbers on the crystalline substrate and spread slowly. This change in secondary nucleation regime

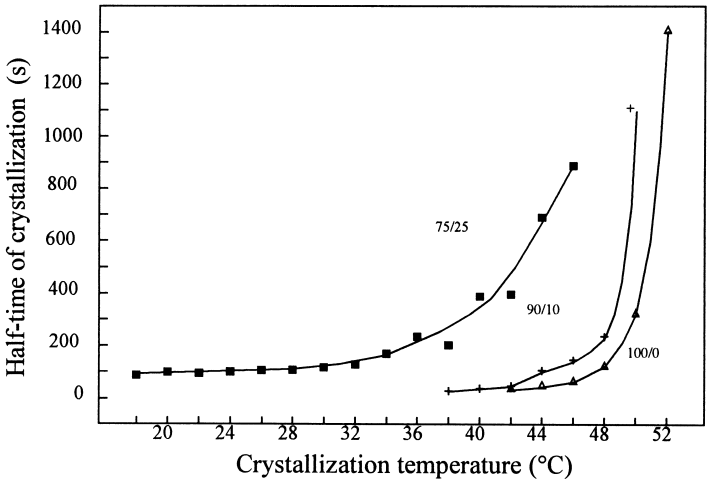

Fig. 5. Half-time of crystallization $t_{1/2}$ versus crystallization temperature T_c for pure PEO, 90/10 and 75/25 PEO/PES blends.

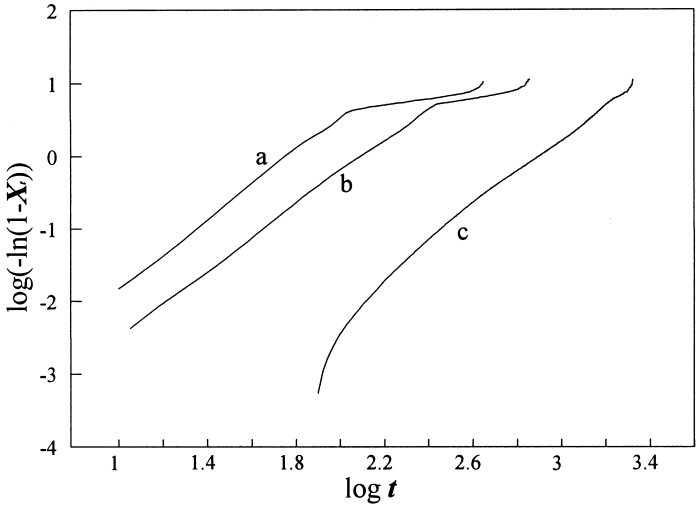

Fig. 6. Avrami-plots for (a) pure PEO, (b) 90/10 and (c) 75/25 PEO/PES blends, crystallized isothermally at 44°C.

from II to III can be inferred from the decreased mobility of PEO chains in the 75/25 PEO/PES blend by which completion of the lamellar surface is retarded in combination with a nearly unchanged formation rate of secondary nuclei.

3.2. Overall crystallization kinetics

The overall crystallization kinetics was investigated by isothermal DSC-experiments. Plots of the half-time of crystallization ($t_{1/2}$) versus T_c for different PEO/PES blend compositions are presented in Fig. 5. The overall crystallization rate increases with decreasing crystallization temperature (T_c) and decreases with a higher amount of PES in the blends. The overall crystallization kinetics is usually described using the Avrami equation [34].

$$\log(-\ln(1 - X_t)) = \log K + n \log(t) \quad (6)$$

where K is the overall crystallization rate constant, t the crystallization time and n the Avrami exponent. Plotting $\log(-\ln(1 - X_t))$ versus $\log t$ gives theoretically a linear correlation; from the intercept and from the slope K and n can be obtained respectively. Theoretically n is 3 for three-dimensional crystallite growth with heterogeneous nucleation and 4 for homogeneous nucleation. In most cases n is a non-integer and as a consequence it is difficult to make straightforward conclusions from it [35]. In our study, information on the presence of different steps in the crystallization process can be derived from Avrami plots. An Avrami-plot of PEO and PEO/PES blends during crystallization at 44°C is presented in Fig. 6. Pure PEO and the PEO/PES 90/10 blend clearly show two linear sections with different slopes; the 75/25 PEO/PES blend shows a constant change of the slope. Avrami-plots of the 75/25 PEO/PES blend, crystallized at lower temperatures (18°C, 28°C and 36°C) show a two-step crystallization process (Fig. 7). The appearance of two linear sections with a different slope at high degree of undercooling can be attributed to primary crystallization followed by a secondary crystallization

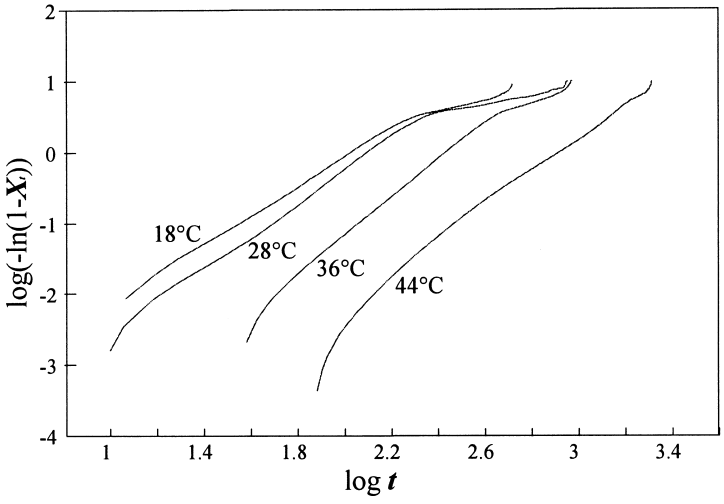

Fig. 7. Avrami-plots for 75/25 PEO/PES blend crystallized isothermally at 18°C, 28°C, 36°C and 44°C.

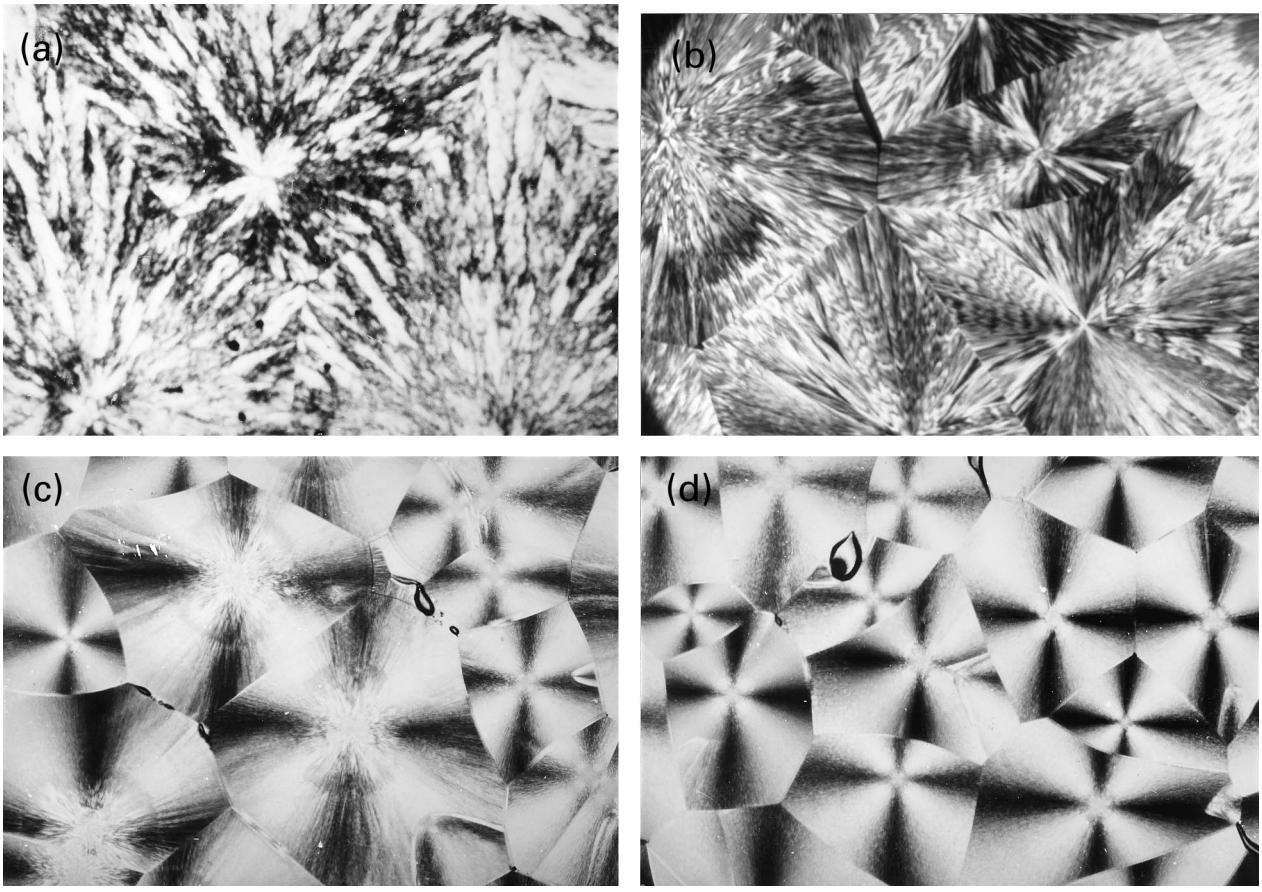

Fig. 8. Optical micrographs under crossed polarizers for PEO/PES blends (a) 100/0, $T_c = 44°C$, (b) 90/10, $T_c = 44°C$, (c) 75/25, $T_c = 44°C$, (d) 75/25, $T_c = 28°C$ (magnification 15 ×).

process [36]. At high temperatures (e.g. 44°C), crystallization of the 75/25 PEO/PES blend is slow, and the secondary crystallization process starts already during the primary one resulting in a continuous changing slope in the Avrami-plot. At lower temperatures (18°C, 28°C and 36°C), the primary crystallization process is fast and the delayed, secondary crystallization of some of the PEO-chains starts only after the end of the primary crystallization. A more detailed discussion on the origin of this secondary crystallization process will be given in the evaluation of the melting behavior.

3.3. Supermolecular structure and segregation behavior of the amorphous component

PEO crystallizes from the melt in a spherulitic, hedritic or intermediate morphology depending on its molecular weight and the crystallization conditions. According to the morphological map presented by Allen and Mandelkern [37] PEO with a molecular weight of 17000 g/mole exhibits a hedritic or an intermediate hedritic-spherulitic morphology depending on the crystallization temperature. This intermediate hedritic-spherulitic morphology was indeed observed by optical microscopy under crossed polarizers for pure PEO crystallized at 44°C (Fig. 8).

The addition of PES to PEO favors the formation of a spherulitic morphology. When the PES content increases to 25 wt.%, PEO crystallizes in a spherulitic morphology at both crystallization temperatures of 28°C and 44°C, showing the typical maltese crosses in Fig. 8(c) and (d). Similar changes in the PEO crystalline morphology have been reported in blends with PVAc [17] and Aramide 34I [21]. Hedrites consist of more or less layered lamellar structures grown from a central screw dislocation; spherulites are lamellar structures that grow spherically in three dimensions. In the 75/25 PEO/PES blend nucleation regime III is occurring, and the higher amount of secondary nuclei favors growth in three dimensions giving rise to spherical morphologies. At a lower amount of PES in the blends, secondary nucleation follows regime II conditions with a smaller amount of growing nuclei and intermediate hedritic-spherulitic morphologies are formed. A similar relationship between the nucleation regime and the crystalline morphology has been reported for linear polyethylene; axialites follow nucleation regime I whereas spherulites follow regime III [27].

The final spherulite size is determined by the ratio of the

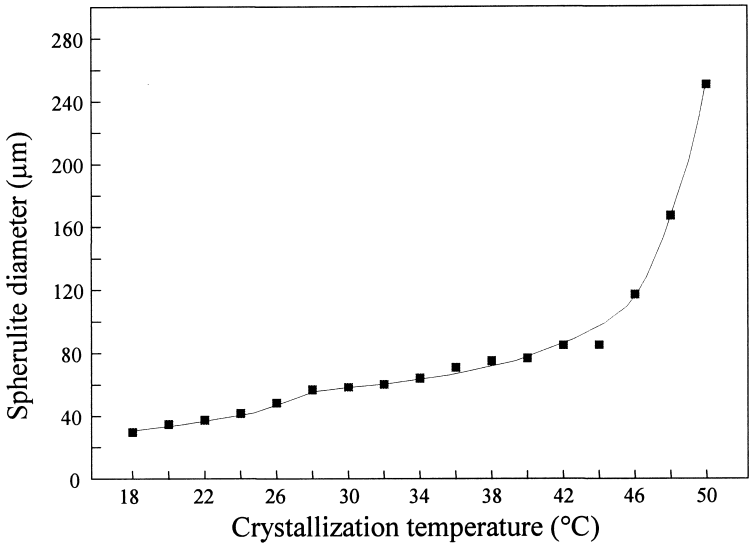

Fig. 9. Spherulite diameter versus crystallization temperature for 75/25 PEO/PES blends.

primary nucleation rate that increases with higher degree of undercooling and the spherulite growth rate, which shows a bell-shaped temperature dependency. The change of the spherulite size with crystallization temperature of isothermally crystallized PEO/PES 75/25 blends is shown in Fig. 9. The spherulite size increases with increasing crystallization temperature; a local maximum in the spherulite dimension curve can be found at 28°C and corresponds with the maximum of the bell-shaped spherulite growth rate curve in Fig. 3.

During crystallization of PEO, the amorphous component PES can segregate into interlamellar, interfibrillar or interspherulitic regions. Fig. 8 reveals that all spherulites are volume filling indicating intraspherulitic segregation of PES. To find out whether the amorphous component PES segregates interlamellar or interfibrillar during crystallization of PEO, SAXS-measurements have been performed on isothermally crystallized PEO/PES blends at 44°C. The long periods, as obtained from Lorentz corrected patterns, are presented in Table 2. With increasing amount of PES, the long period increases revealing interlamellar segregation of PES during crystallization of PEO. It has been pointed out [38] that the scale of segregation of the amorphous component during crystallization is related to the ratio between the diffusion rate D of the amorphous component and the growth rate G of the crystalline component. The segregation behavior of several amorphous components with different glass-transition temperatures and types of interactions in PEO blends was recently investigated [20]. It was concluded that although the effect of mobility of the diluent cannot be neglected, it is mainly the growth rate of the PEO crystals that dominates the length scale of segregation. In the present study the amorphous component PES has a high T_g and consequently the mobility of the amorphous component decreases at higher PES content in the blends. A strong decrease of the spherulite growth rate of PEO with increasing PES content has been observed and was mainly attributed to the decreased mobility of PEO on adding amorphous PES component. From our experiments it can be concluded that in blends containing up to 25 wt.% PES, PES segregates interlamellarly. Aramide 34I also segregates interlamellarly in blends with PEO [21]. The interlamellar segregation of these high T_g amorphous components means that the strong decrease in the PEO spherulite growth rate in PEO/PES and PEO/Aramide blends is accompanied by a low diffusion rate of the amorphous component. As a consequence both the diffusion rate of the amorphous component and the spherulite growth rate determine the segregation behavior.

Table 2
Long period and PEO degree of crystallinity of PEO/PES blends, crystallized isothermally at 44°C for 1 h

PEO/PES composition	Long period L (Å)	Crystallinity X_c (%)
100/0	167	96
90/10	144	96
80/20	223	91
75/25	273	88
60/40	478	57

3.4. Melting behavior

The melting behavior of isothermally crystallized PEO/PES blends was investigated using DSC. Melting thermograms of PEO, 90/10 and 75/25 PEO/PES blends isothermally crystallized at 44°C for 24 h are presented in Fig. 10. PEO crystals melt at 65°C; with increasing amount of PES in the blends a melting point depression for the highest melting peak is present and a second melting endotherm appears at lower temperatures. The occurrence of multiple melting in a blend of an amorphous and a semi-crystalline component has been attributed by Groeninckx et al. to

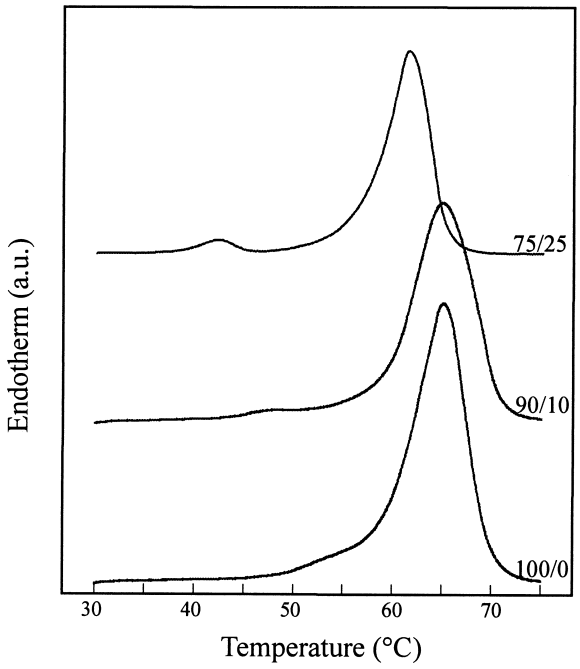

Fig. 10. DSC heating curves at 10°/min of pure PEO and PEO/PES blends, isothermally crystallized at 44°C for 24 h.

different processes [39–41], including recrystallization and secondary crystallization.

Several experiments were performed to identify the origin of the double melting behavior of the PEO/PES blend system. The 75/25 PEO/PES blend was isothermally crystallized at 28°C for different times (from 300 s to 73 h) and subsequently melted in the DSC (Fig. 11). The higher melting endotherm at 62°C is constant with increasing crystallization time. A smaller melting peak appears at 38°C after 10 min crystallization that increases and shifts to higher temperature with longer crystallization times. This lower melting endotherm is absent in the DSC-curve after crystallization for 200 s, the time period after which a change of the slope of the Avrami-plot appeared (see Fig. 7). Apparently some PEO-chains show retarded, secondary crystallization and lamellar thickening after the primary crystallization process and melt at lower temperatures than the primary formed lamellae. This observation confirms that the change of the slope in the Avrami-plot is related to the start of the secondary crystallization process.

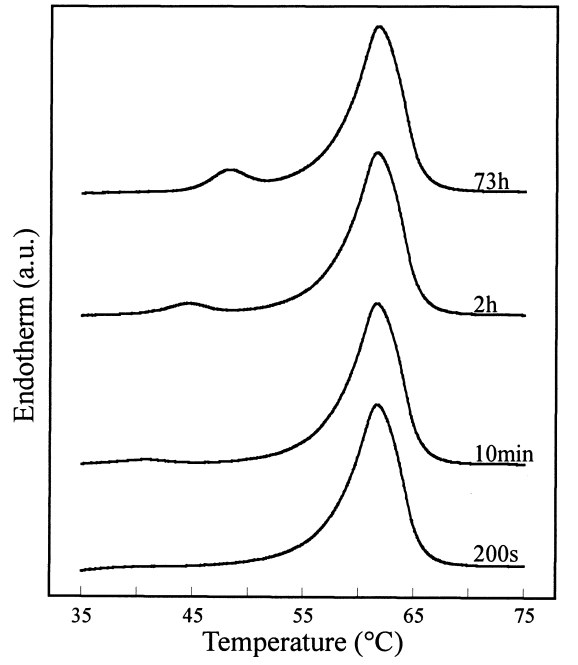

Fig. 11. DSC heating curves at 10°/min of 75/25 PEO/PES blend, isothermally crystallized at 28°C for different times.

To investigate recrystallization of the 75/25 PEO/PES blend, DSC-measurements at different heating rates between 1 and 40°C/min were carried on samples crystallized at 24°C for 60 min, as shown in Fig. 12(a). At low heating rates a very small lower melting endotherm is present. This lower endotherm moves to higher temperatures and becomes more important at higher heating rates compared to the higher melting endotherm. The higher melting peak shifts slightly to lower temperatures with increasing heating rate from 1.5 to 10°/min. The broadening and shift to higher temperatures of this endotherm at heating rates of 20 and 40°/min must be interpreted as an artifact and can be assigned to thermal lag of the sample.

After primary crystallization of PEO, a secondary crystallization process starts during which thin lamellae melting at lower temperatures are formed. As a consequence, two types of lamellae are present in the crystalline 75/25 PEO/PES blend. During heating at low heating rates the thin secondary lamellae melt first and recrystallize by which the resulting lower melting endotherm decreases and shifts to lower temperatures, as illustrated in Fig. 13(a). The recrystallized lamellae melt at a slightly higher temperature than the thick primary lamellae resulting in a shift to higher temperature and an increase in intensity of the higher melting endotherm compared to DSC-curves obtained at higher heating rates where less recrystallization occurs.

A 50/50 PEO/PES blend requires a longer crystallization time than the 75/25 PEO/PES blend. DSC melting curves at different heating rates of a 50/50 PEO/PES blend after crystallization at 28°C for 450 h are presented in Fig. 12(b). The DSC-thermograms show that the lower melting endotherm moves towards the higher melting endotherm and increases in intensity compared to the higher melting endotherm at increasing heating rates from 1.5 to 20°/min. The higher melting endotherm decreases in intensity and shifts slightly to lower temperatures. At a heating rate of 40°C/min one broad melting endotherm is present. As a result of thermal lag of the sample at 20 and 40°/min an additional shift of the melting peaks is present.

From these results can it be concluded that the 50/50 PEO/PES blend forms only one type of lamellae with a broad distribution in lamellar thickness during the

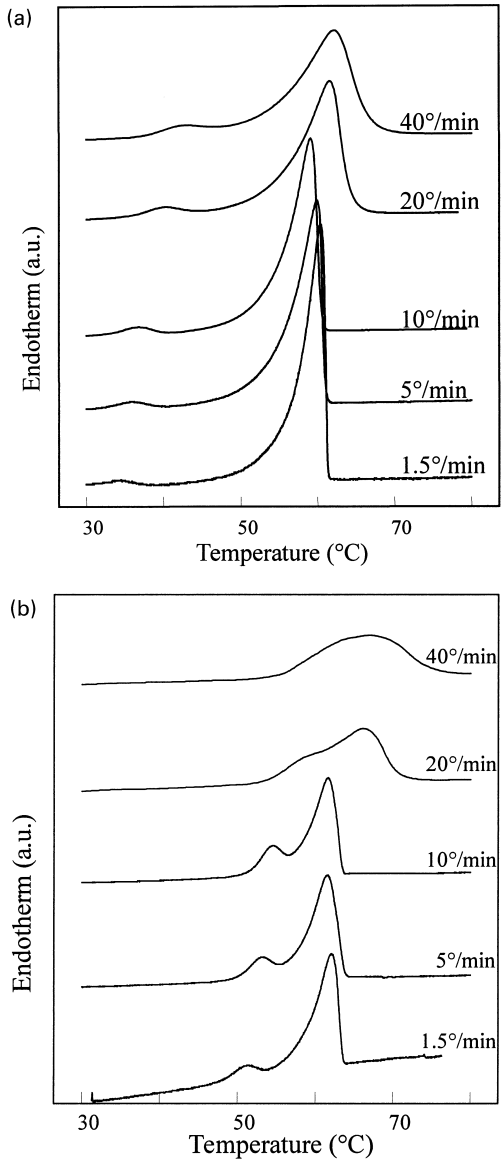

Fig. 12. DSC heating curves at different heating rates of (a) 75/25 PEO/PES blend crystallized at 24°C for 1 h, (b) 50/50 PEO/PES blend crystallized at 28°C for 450 h.

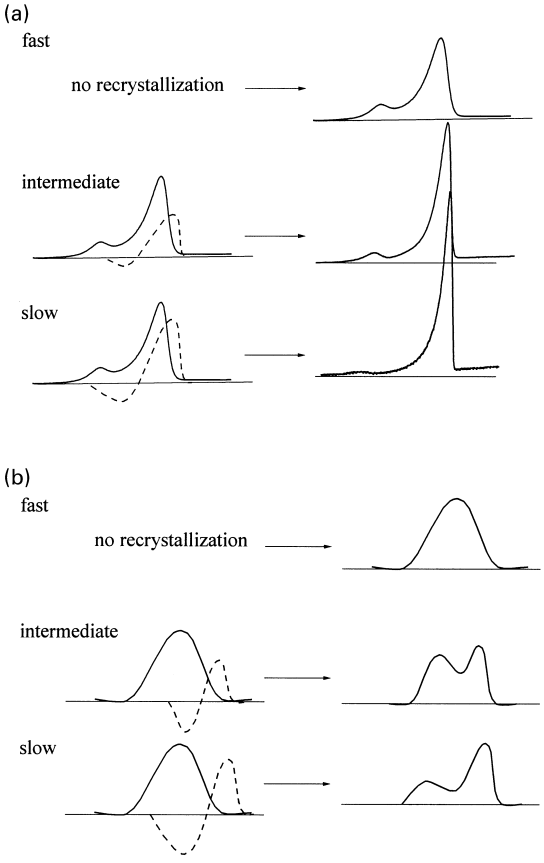

Fig. 13. Model describing the influence of recrystallization/remelting phenomena on the DSC heating curves of (a) 75/25 PEO/PES blend where initially two types of lamellae are present, (b) 50/50 PEO/PES blend where initially one type of lamellae is present.

isothermal crystallization process. A 50/50 PEO/PES blend crystallizes much slower than a 75/25 blend and forms one type of lamellae, the remaining amorphous phase contains a high amount of PES that inhibits further secondary crystallization. The observed double melting behavior of the 50/50 PEO/PES blends is attributed to a recrystallization/remelting phenomenon. At low heating rates lamellae melt, recrystallize and remelt again at higher temperatures. The observed double melting endotherm is the superposition of these processes; a model representation of this phenomenon is given in Fig. 13(b). With increasing heating rate a smaller fraction of the lamellae is able to recrystallize and the two melting endotherms shift towards each other. At high heating rates none or only a small amount of lamellae recrystallizes leading to a broad melting endotherm.

The degree of crystallinity of PEO/PES blends crystallized at 44°C for 1 h are presented in Table 2. The crystallinity of PEO in the blends decreases from 96% for pure PEO to 57% in the 60/40 PEO/PES blends indicating a pronounced influence of the amorphous component PES on the final crystallinity of PEO. The high crystallinity of PEO has to be assigned to the use of the temperature dependent enthalpy function, the degree of crystallinity of PEO obtained after dividing the melting enthalpy by 196.4 J/g is 86%.

4. Conclusions

The crystallization kinetics of PEO in miscible binary blends with PES are strongly affected by the presence of the amorphous component; both the overall crystallization rate and the spherulite growth rate show a pronounced decrease. The changes in the crystallization behavior are related to the lower mobility of PEO in the blends with PES, which in turn is related to the high T_g of PES. The

variation of the secondary nucleation regime is reflected in the final supermolecular morphology of the PEO/PES blends that changes from intermediate hedritic-spherulitic to spherulitic. During crystallization of PEO the amorphous component PES segregates into the interlamellar regions.

The melting behavior of these blends is complex and can be interpreted in terms of both secondary crystallization and recrystallization. At small amounts of PES, a small fraction of PEO molecules shows secondary crystallization and the blend consists of thin secondary lamellae and thicker primary lamellae. Upon melting the secondary lamellae recrystallize and melt at higher temperature. A different semi-crystalline morphology is proposed for 50/50 PEO/PES blend; on account of the slow primary crystallization process no additional secondary crystallization occurs. During heating, the lamellae recrystallize and the 50/50 PEO/PES blend exhibits as well a double melting behavior.

Acknowledgements

This research was financially supported by the Research Council K.U. Leuven and the Fund for Scientific Research Flanders (FWO-Vlaanderen). One of the authors (G. Dreezen) is indebted to the Flemish Institute for the promotion of Scientific-Technological Research in Industry (I.W.T.) for a fellowship.

References

[1] Tanaka H, Nishi T. Physical Review A 1989;39(2):783.
[2] Li Y. Stein M. Jungnickel, B-J. Colloid Polym Sci 1991;269:772.
[3] Shibanov YuD, Godovsky YuK. Progr Colloid and Polymer Sci 1989;80:110.
[4] Li Y, Schneider L, Jungnickel B-J. Polym Networks Blends 1992;2(3):135.
[5] Delimoy D, Goffaux B, Devaux J. Legras R. Polymer 1995;36(17):3255.
[6] Shibanov Y, Godovsky Y. Progr Colloid and Polymer Sci 1989;80:110.
[7] Schulze K, Kressler J, Kammer H. Polymer 1993;34:3704.
[8] Cham PM, Lee TH, Marand H. Macromolecules 1994;27:4263.
[9] Inaba N, Yamada T, Suzuki S, Hashimoto T. Macromolecules 1988;21:407.
[10] Li Y, Jungnickel B-J. Polymer 1993;34:9.
[11] Wellscheid R, Wüst J, Jungnickel B-J. J Polym Sci part B: Polym Phys 1996;34:267.
[12] Walsh D, Singh V. Makromol Chem 1984;185:1979.
[13] Guo W, Higgins J. Polymer 1990;31:699.
[14] Martuscelli E, Silvestre C, Gismondi C. Makromol Chem 1985;186:2161.
[15] Martuscelli E, Silvestre C, Addonizio ML, Amelino L. Makromol Chem 1986;187:1557.
[16] Silvestre C, Cimmino S, Martuscelli E, Karasz FE, Macknight WJ. Polymer 1987;28:1190.
[17] Silvestre C, Karasz FE, Macknight WJ, Martuscelli E. Eur Polym J 1987;23:745.
[18] Cimmino S, Martuscelli E, Silvestre C, Canetti M, de Lalla C, Seves A. J Polym Sci: B: Polym Phys 1989;27:1781.
[19] Alfonso G, Russell T. Macromolecules 1986;19:1143.
[20] Talibuddin S, Wu L, Runt J, Lin JS. Macromolecules 1996;29:7527.
[21] Dreezen G, Koch MHJ, Reynaers H, Groeninckx G (submitted to Polymer).
[22] Mathot VBF, Calorimetry and Thermal Analysis of Polymers' Mathot VBF, editor, Hanser Publishers, 1994, Ch.5, 105–167; Ch.9, 231–299.
[23] Gaur U, Lau SF, Shu HC, Wunderlich BB. J Phys Chem Ref Data, 10 (1981) 89, 119, 1001; 11 (1982) 313, 1065; 11 (1982) 313, 1065; 12 (1983) 29, 65, 91.
[24] Varma-Nair M, Wunderlich BB, Mehta A. J Phys Chem Ref Data 1991;20(2):349.
[25] Vonk CG. J Appl Cryst 1975;8:340.
[26] Fox TG. Bull Am Phys Soc 1956;2:1123.
[27] Hoffman JD, Davis GT, Lauritzen JI, Treatise on Solid State Chemistry Hannay NB, editor, New York: Plenum, 1976, Vol 3, Chap 7.
[28] Turnbull D, Fisher JC. J Chem Phys 1949;17:71.
[29] Chow TS. Macromolecules 1990;23:333.
[30] Calahorra E, Cortazar M, Guzman GM. Polymer 1982;23:1322.
[31] Martuscelli E, Pracella M, Yue WP. Polymer 1984;25:1097.
[32] Lauritzen JI, Hoffman JD. J Appl Phys 1973;44:4340.
[33] Arlie JP, Spegt P, Skoulios A. Makromol Chem 1967;104:212.
[34] Avrami MJ. Chem Phys 1939;7:1103.
[35] Grenier D, Prud'homme RE. J Polym Sci, Polym Phys Ed 1980;B18:1655.
[36] Price F. J Polym Sci Part A 1965;3:3079.
[37] Allen C, Mandelkern L. J Polym Sci Part B: Polym Phys 1982;20:1465.
[38] Keith HD, Padden FJ. J Polym Sci; Polym Phys Ed 1987;25:229.
[39] Defieuw G, Groeninckx G, Reynaers H. Polymer 1989;30:2158.
[40] Defieuw G, Groeninckx G, Reynaers H. Polymer 1989;30:2164.
[41] Vanneste M, Groeninckx G. Polymer 1994;35:1051.